Journal of Colloid and Interface Science 466 (2016) 227–237

Contents lists available at ScienceDirect

Journal of Colloid and Interface Science

journal homepage: www.elsevier.com/locate/jcis

Sonosynthesis of an Ag/AgBr/Graphene-oxide nanocomposite as a solar photocatalyst for efficient degradation of methyl orange

A. Esmaeili [a], M.H. Entezari [a,b,*]

[a] Sonochemical Research Center, Department of Chemistry, Faculty of Science, Ferdowsi University of Mashhad, 91779 Mashhad, Iran
[b] Environmental Chemistry Research Center, Department of Chemistry, Faculty of Science, Ferdowsi University of Mashhad, 91779 Mashhad, Iran

GRAPHICAL ABSTRACT

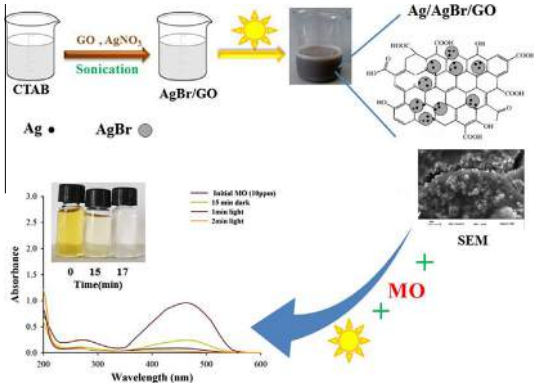

ARTICLE INFO

Article history:
Received 5 November 2015
Revised 14 December 2015
Accepted 17 December 2015
Available online 18 December 2015

Keywords:
Ag/AgBr/GO
Ultrasound irradiation
Photocatalytic activity
Sunlight
MO degradation

ABSTRACT

In this study, a new method has developed for the synthesis of Ag/AgBr/Graphene-oxide (Ag/AgBr/GO) nanocomposite with high adsorption capacity and high photocatalytic activity in degradation of methyl orange (MO). In this method, ultrasound was applied in the synthesis and it was facilitated the process. The samples prepared under ultrasound were shown as Ag/AgBr/GO-U, and the samples under conventional method as Ag/AgBr/GO-C. The results of FT-IR, XRD, Raman, DRS and SEM confirmed the structure of the nanocomposites very well. Ultrasound played a key role in the formation of nanocomposite with smaller size of GO sheets and particles. Different amount of GO was used in the nanocomposite composition and their photocatalytic activities were compared. The MO in solution was completely degraded in 15 min, 30 min, and 45 min with Ag/AgBr/GO-U-1 that contained 1 mg mL^{-1} GO, Ag/AgBr/GO-U-0.5 that contained 0.5 mg mL^{-1} GO and Ag/AgBr/GO-C-0.5 that contained 0.5 mg mL^{-1} GO, respectively. The chemical oxygen demand (COD) measurements displayed a complete mineralization in 30 min for Ag/AgBr/GO-U-0.5. The data obtained from the degradation experiments were fitted to the first-order kinetics and the adsorption obeyed the Langmuir model. The nanocatalyst did not exhibit significant loss of activity even after four cycles of successive uses. To determine the mechanism of photocatalytic degradation of MO, different scavengers were used. Based on the results, the superoxide radical, hydroxyl radical and hole had a key role in the degradation process. The Ag/AgBr/GO-U-1 nanocomposite exhibited the highest photocatalytic activity due to its high adsorption capacity and enhanced charge transfer.

* Corresponding author at: Sonochemical Research Center, Environmental Chemistry Research Center, Department of Chemistry, Faculty of Science, Ferdowsi University of Mashhad, 91779 Mashhad, Iran.
E-mail addresses: entezari@um.ac.ir, moh_entezari@yahoo.com (M.H. Entezari).

http://dx.doi.org/10.1016/j.jcis.2015.12.034
0021-9797/

1. Introduction

In recent years, different kinds of aromatic compounds, organic dyes and pharmaceutical pollutant produced from industry, textile, agriculture and waste processes have a negative impact on humans and the ecosystems. To solve these problems, great hard works have been dedicated to develop photocatalysts to achieve the photodegradation of the pollutants. Applying semiconductor photocatalysts to decompose organic pollutant in air and water is a possible approach for solving environmental problems [1–3]. Semiconductor photocatalysis has attracted increasing interest as a green technology to solve the existing energy and environmental problems of human society [4,5]. TiO_2, a conventional photocatalyst, cannot be broadly used in practical applications because of low photocatalytic efficiency on sun light and its limited visible-light absorption [6–9]. In the other hand, sunlight is the best energy source for the action of photocatalysts. Thus, it is highly required to extend new, stable, efficient, and sun -light photocatalysts. Strong visible light absorption was shown by noble metal nanoparticles (for example Au, Ag and Pt). It is due to surface plasmon resonance (SPR) of these particles [10,11]. As outcome, plasmonic noble metal nanoparticles can be used to enhance the visible light absorption of photocatalysts [12–16]. Recently, Ag/AgX (X = Cl, Br, I) has attracted a lot of attention for photocatalytic activity because of its capability in absorption of visible light due to surface plasmon resonance effect. However, AgX has the main role in the degradation of pharmaceutical pollutant, dye pollutant and bacteria due to photoactive species [17–19]. Also, it was realized that the Ag/AgBr could not use the whole photoactivity because of its large particles [20,21]. The hybrid materials can improve the Ag/AgX dispersion in medium that can enhance electron transfer in substrate and better photocatalytic activity [22].

Different methods have been used to modify Ag/AgX to enhance its photocatalytic activity. CNTs were used by Li et al. to modify Ag/AgBr, and their results showed an improvement in photocatalytic activity [23–26].

Graphene oxide (GO), an atomic thick nanosheet of covalently organized two-dimensional lattice of carbon atoms that decorated with different oxygen-containing groups such as hydroxyl, epoxide, carbonyl and carboxyl, has newly received considerable attention as a novel kind of graphene [27–29]. Some properties of GO, such as hydrophilicity and nice solubility in solvents caused to use GO for the production of GO-based hybrid nanocomposites. These nanocomposites have been applied for different applications such as chemical and biochemical sensors, drug delivery, electrochemical field and high efficiency catalysis [30–32]. Currently fabrication of GO-involved catalyst especially for the photodegradation of pollutants much attention has received. High specific surface area, locally conjugated aromatic system, and unique electronic properties of the graphene-based materials, making them ideal candidates for catalyst with excellent efficient and strong photocatalysts [33,34]. So coupling GO with Ag/AgBr is an effective strategy to improve efficiency of photocatalytic activity for degradation of pollutant.

After selecting the appropriate catalyst synthesis is the next important issue, there are different methods for the synthesis Ag/AgBr like ion exchange, precipitation etc. that needs long time or difficult conditions. Consequently, a more facile method is strongly required.

The sonochemical method can be used to obtain nanocomposites [35,36]. The high-intensity ultrasound irradiation in liquid solutions creates the acoustic cavitation effect, collapse of bubbles and high temperatures and pressures in small regions of the solution that all these effects result in high speed, simple condition of synthesis and better quality of products [37,38]. In this work, ultrasound irradiation has been applied in the preparation of Ag/AgBr/GO nanocomposite for the photocatalytic applications. The sonosynthesis nanocomposite was carried out in a short time under mild conditions. The complete degradation of Methyl orange (MO) was approved in the presence of Ag/AgBr/GO nanocomposite under sun light irradiation.

2. Experimental

2.1. Materials

Graphite powder (purity 99%, mesh 325), potassium permanganate (KMnO4), sodium nitrate ($NaNO_3$), sulfuric acid (H_2SO_4), hydrochloric acid (HCl), hydrogen peroxide (H_2O_2), silver nitrate ($AgNO_3$, 99%), cetyltrimethyl ammonium bromide (CTAB) were obtained from Merck. All materials were used as received without additional purification or treatment. Methyl orange (MO) from Aldrich, were used as received. De-ionized water (DI) was used in the synthesis of the GO.

2.2. Preparation of GO

GO was prepared by the ultrasonic method [39]. In a usual procedure, 0.5 g graphite powder and 0.5 g $NaNO_3$ were added into 23 mL H_2SO_4. The mixture stirred in an ice bath. 3.0 g $KMnO_4$ was added to mixture little by little in the next step. Then, the suspension was irradiated for 20 min in ultrasonic bath at room temperature. The prepared suspension was diluted by 40 mL deionized water. At least, with adding 100 mL de ionized water and 3 mL H_2O_2 (30%) to the suspension the process was finished. The mixture was filtered and washed with HCl aqueous solution and distilled water and dried under vacuum at 80 °C for 24 h. To obtain GO nanosheets as a dispersed phase in water, 50 mg of as-synthesized dried solid product was added to 50 mL of distilled water and then sonicated with an ultrasonic homogenizerfor1 h.

2.3. Preparation of Ag/AgBr/GO

Ag/AgBr/GO was synthesized via a facile and fast ultrasonic method. In a typical procedure, 20 mL aqueous solution of GO (1 mg mL^{-1}) was added to 50 mL cetyltrimethyl ammonium bromide (CTAB) aqueous solution (0.015 M) with vigorous stirring for 10 min and then 50 mL of a 0.015 M $AgNO_3$ aqueous solution was added drop by drop. At next step the mixture was sonicated with probe ultrasonic for 30 min (at classic procedure mixture was lasted for several hours for example 6 h in [40] and 24 h in [33]) at room temperature to preparation AgBr/GO. Finally, to synthesize Ag/AgBr/GO we need UV light to produce Ag nano particle on AgBr/GO composite. Generally, UV lamp was used to this reduction [33,40,41]. In this work, without any special lamp, the mixture was irradiated under sunlight for 30 min to produce Ag/AgBr/GO–U. The color of the product changed to grey, which indicated that silver nanoparticles were produced. The product was collected and washed with distilled water and absolute ethanol 2–3 times. Ag/AgBr/GO-C synthesized with stirring for 3 h instead of ultrasonic irradiation and Ag/AgBr nanocomposite was also synthesized via a parallel process without the introduction of GO.

2.4. Photocatalytic performance of the samples

In photocatalytic degradation experiments, direct sunlight was applied as an energy source. The catalytic activity of as prepared Ag/AgBr/GOs nanocomposites have been studied for the photocatalytic degradation of MO in an aqueous solution. In these tests, 25 mL MO (10 mg L^{-1}) and 0.015 g of each catalyst at natural pH were added to the Pyrex glass vessel and magnetically were stirred.

Different stirrer were employed in identical rate of stirring and at fix interval time under direct solar radiation in following sunny days in the range of 10 am–2 pm on the edge of window (GPS coordinates: N = 36_18041.600, E = 59_31054.200). The temperature of the solution was between 17 and 20 °C. Before beginning photocatalytic activity under sunlight irradiation, the solutions were magnetically stirred in a dark place to achieve adsorption–desorption equilibrium between the MO and photocatalyst. The experiments were performed in different times and to attain equilibrium, 15 min was needed. Different amounts of catalyst (0.40 g L^{-1}, 0.60 g L^{-1}, 0.8 g L^{-1}, 1.00 g L^{-1}) were checked, 0.6 g L^{-1} was the best choice for dosage of catalyst. The turbidity of the suspension was increased by increasing the amount of catalyst, and this led to the decrease of light scattering and diffusion of light. At determinate interval times, about 5 mL of suspensions were separated by centrifuge. The removal of MO was determined based on the absorption at 465 nm by using a UV–vis spectrophotometer. Then, the absorption was transformed to concentration through the standard curve of MO. Dichromate method was used to determine the chemical oxygen demand (COD) of the samples [42] after solution centrifuge. The experiments were done under sun light irradiation for the samples Ag/AgBr/GO-C and Ag/AgBr and the results showed that the best yield of decomposition was attained for the Ag/AgBr/GO-U nanocomposite. Hence, the sono-synthesized nanocomposite as aphotocatalyst was selected for the degradation of the pollutant.

2.5. Characterization and equipment

The structure, morphology, and light absorption properties of the as-prepared nanocomposites were characterized by using Fourier-transformed infrared spectroscopy (FT-IR), X-ray diffraction (XRD), Scanning electron microscopy (SEM), UV–Vis diffuse reflection spectroscopy (DRS) and Raman spectroscopy. The FTIR were recorded on a Thermo Nicolet 370 spectrometer, the spectrum was obtained by mixing the sample with KBr. XRD was performed in a wide range angle (2θ = 4°–80°) by Bruker-axs, D8 Advance model at a scanning rate of 0.06°/s, with monochromatized CuKα radiation (λ = 1.5406 Å). DRS was analyzed by MC-2530. SEM was performed with LEO 1450VP. Raman spectroscopy was done with an Almega Thermo Nicolet Dispersive Raman Spectrometer with a 532 nm laser excitation. To determine the concentration of MO in solution, UV–Vis adsorption spectra were recorded by the UV–Vis spectroscopy (Unico 2800). The ultrasonic irradiation was applied with equipment operating at 20 kHz (Branson Digital Sonifier, W-450 D) and bath ultrasound (Branson, model 8510E-DTH, USA, 40 kHz, 250 W).

3. Results and discussion

3.1. Characterization of the catalyst

Practically, as shown in Fig. 1, the Ag/AgBr/GO nanocomposites could be successfully fabricated by adding GO and $AgNO_3$ aqueous solution to CTAB aqueous solution and following by ultrasonic irradiation. The functional groups like hydroxyl, epoxide and carboxylic on GO sheets could act as good attaching sites for the nucleation and growth of AgBr nanoparticles [33]. Few amount of Ag^+ in AgBr are converted into Ag nanocrystals by the ambient light through the AgBr growth process on GO nanosheets. Whereas under the subsequent sunlight irradiation, more Ag^+ are converted.

In order to investigate the hybridization of Ag/AgBr with GO in Ag/AgBr/GO-U sample, the Fourier transform infrared spectra (FT-IR) of the Ag/AgBr/GO-U sample and GO were recorded as shown in Fig. 2. It could be seen that the GO shows several characteristic peaks at 1731, 1620, 1222, and1051 cm^{-1}, which are attributed to the C=O carbonyl stretching, the O—H deformation vibration, and the C—OH and C—O stretching, respectively [39]. The C=O carbonyl stretching band at 1731 cm^{-1}in GO shifts to lower wavenumber, 1712 cm^{-1}, in Ag/AgBr/GO-U sample, that represent the obvious interactions between the Ag/AgBr nanoparticles and GO nanosheet [34]. In addition, the intensity of carbonyl stretching band in Ag/AgBr/GO-U was weaker compared with GO. Therefore, hybridization between GO nanosheets and Ag/AgBr nanoparticles was confirmed by FT-IR results.

Distinct absorption in the visible region has key role for the visible-light and sunlight energized catalysts. Totally, pure AgBr species could only display distinct absorption in the ultraviolet region but not strong absorption in the visible region [25,43]. Whereas, the as-prepared nanocomposites Ag/AgBr/GO-U and Ag/AgBr/GO-C show strong absorption both in the UV and visible regions as shown in Fig. 3. This proposed the existence of metallic Ag particles in all samples, which could produce SPR absorptions in the visible region [44]. It means the optical properties of plasmonic noble metal are dominated by their SPR when excited by irradiative light with a specific wavelength. This exciting was occurred with adsorption light in visible, IR and NIR regions. Also, Ag/AgBr/GO-U nanocomposite shows stronger absorption in visible region compared with Ag/AgBr/GO-C that refers to more presence of GO and Ag nanoparticles in Ag/AgBr/GO-U. Therefore, the as-prepared photocatalysts especially Ag/AgBr/GO-U has higher photocatalytic activity in the whole sunlight region.

The crystal structures and existence of metallic Ag in as-prepared nanocomposites could be established by the XRD investigation. As shown in Fig. 4, the XRD pattern of Ag/AgBr/GO-U, Ag/AgBr/GO-C and Ag/AgBr indicated distinct diffraction peaks that are attributed to cubic phase of AgBr (JCPDS file: 6-438) and metallic Ag (JCPDS file: 4-783), that included 2θ at 26.7° (111), 30.9° (200), 44.3° (220), 52.5° (311), 55.0° (222), 64.5° (400), 71.1° (331), 73.2° (420) for AgBr, and 38.2° (111), 44.3° (200), 64.5° (220), 77.9° (311) due to presence of Ag [45]. This result confirms the presence of metallic Ag in nanocomposites and it suggests the formation of Ag/AgBr-based nanocomposites. However, no obvious peaks for GO are observed in the composites by XRD, because when GO is hybridized with inorganic components, the diffraction peak ascribing to GO could hardly be seen by XRD. This is due to the low diffraction intensity of GO nanosheet. Compared with Ag/AgBr, Ag/AgBr/GO-U and Ag/AgBr/GO-C, the peak intensity of Ag in Ag/AgBr/GO-U is stronger, indicating that in the same condition more Ag nanocrystals generate.

Furthermore, the structural change and the interaction effect between GO and Ag/AgBr in Ag/AgBr/GO-U was investigated by the Raman spectra. Totally, graphene oxide nanosheets have two characteristic peaks namely D and G band in the Raman spectrum. The G-band of GO shifts to higher frequency when hybridized with an electron acceptor component and to lower frequencies when hybridized with an electron donor component [34]. As shown in Fig. 5, the D and G band of graphene oxide were also observed in Ag/AgBr/GO-U at 1350 cm^{-1} and1590 cm^{-1}, respectively [33]. Comparison with the G-band of the pure GO nanosheets that placed at ca. 1600 cm^{-1}, a shift by 10 cm^{-1} to a lower frequency, 1590 cm^{-1}, was observed in Ag/AgBr/GO-U. This result confirms very well the composition of GO where Ag/AgBr and GO work as electron donor and electron acceptor, respectively. Additionally, the decrease in the average size of the in-plane sp^2 domains of C atoms in the as-prepared Ag/AgBr/GO-U nanocomposite was indicated by intensity ratio of D-band to G-band (I_D/I_G) in the Raman spectrum which increased from 1.05 for GO to 1.25 for Ag/AgBr/GO-U.

The morphologies of the as-synthesized nanocomposites via ultrasonic and classic methods are characterized by scanning electron microscopy (SEM) as shown in Fig. 6. The sheets of GO were

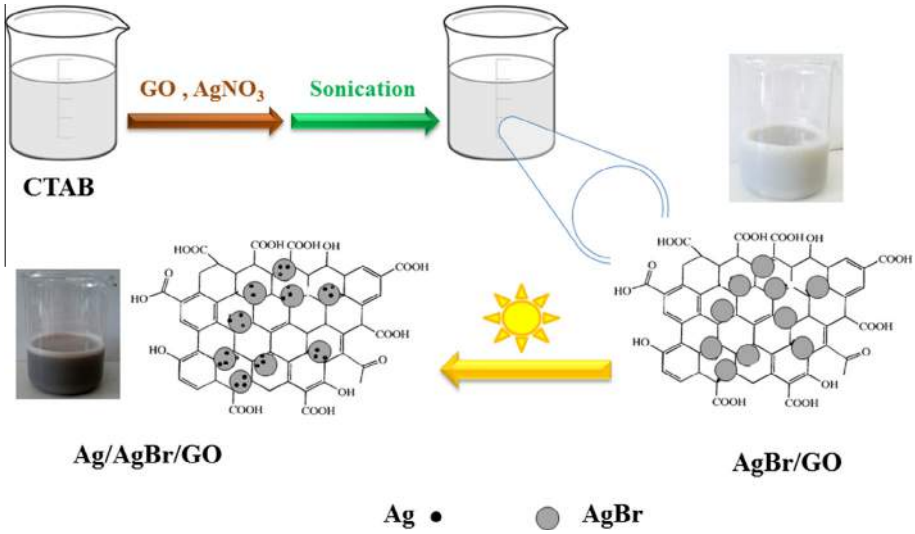

Fig. 1. Schematic Explanation for Ag/AgBr/GO-U nanocomposite.

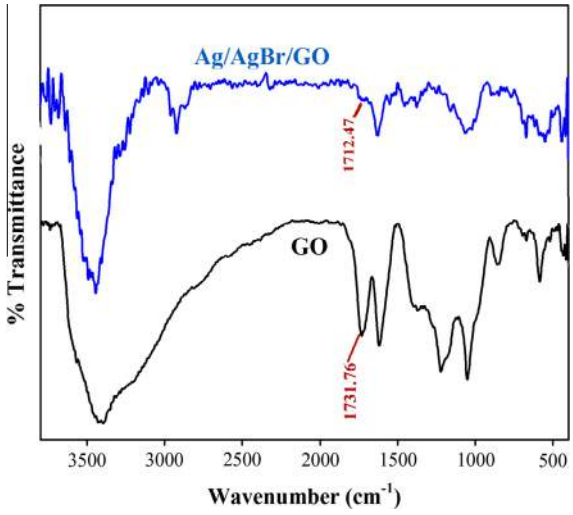

Fig. 2. FT-IR spectrum of GO and Ag/AgBr/GO-U nanocomposite.

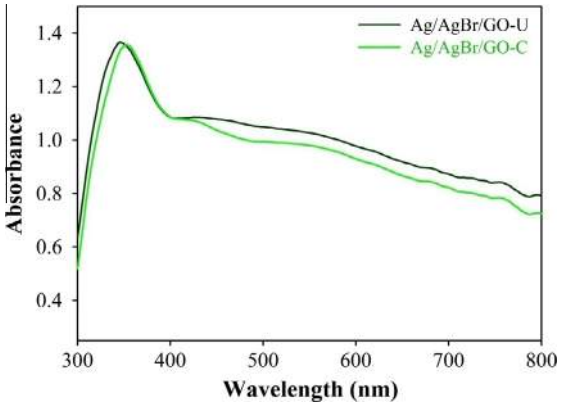

Fig. 3. UV–Vis diffusive reflection spectra of Ag/AgBr/GO-U and Ag/AgBr/GO-C.

observed very well in Fig. 6(b and c) in comparison with Ag/AgBr (Fig. 6a) with no GO sheets. The nanoparticles with an average size of ca. 200–250 nm were obtained when GO was used in nanocomposite (Fig. 6(b and c)). In addition, the Ag/AgBr nanoparticles are smaller in the sample prepared by ultrasound than classical method and this is due to the cavitation process in ultrasonic method. It can be seen from Fig. 6c that nanoparticles penetrate between GO layers and intercalation was occurred in ultrasonic sample. Ag/AgBr nanoparticles that attached onto GO sheets can prevent GO sheets from aggregation and restacking, and both faces of GO sheets are accessible in their application.

Ag/AgBr/GO-U with uniform size of nanoparticles, well distribution of particles on GO, smaller size of GO sheets and intercalation of particles between GO layers, has unique structure which could promote electron transfer of the catalysts in photocatalytic reaction and favorably improve the adsorption capacity of Ag/AgBr/GO due to its high surface area.

3.2. Removal of MO by Ag/AgBr/GO

In the absence of photocatalyst (Ag/AgBr/GO), the photolysis of MO in aqueous solution (10 mg L^{-1}) under direct sunlight irradiation was tested. It was found that no considerable changes observed on the concentration of MO after sunlight irradiation. This indicates that MO is stable and cannot be simply degraded by sunlight irradiation. Then, Ag/AgBr/GO nanocomposites as photocatalyst were applied to investigate MO degradation. In this study, the MO solution with nanocomposite was magnetically stirring in the dark place for different interval times to reach adsorption–desorption equilibrium between the dye (MO) and photocatalyst. 15 min was the optimum time to attain this equilibrium. The suspension after dark step was placed under direct sunlight irradiation for several interval time and studied the photocatalyst effect of nanocomposite on MO degradation. For comparison, the same photocatalytic degradation experiments were performed with Ag/AgBr/GO-U and Ag/AgBr/GO-C. Although Ag/AgBr/GO nanocomposites were synthesized in harder conditions in classic than ultrasonic method, but the sample synthesized with ultrasound exhibited a higher photocatalytic activity (Fig. 7). Through the acoustic cavitation process, collapse of the bubbles caused to very high pressures, temperatures and cooling rates [46] that makes available a favorable situation for the growth of the Ag/AgBr nanocrystals on GO nanosheets. Therefore, in the presence of ultrasound the smaller size of the GO nanosheets with higher surface area can be achieved. In Ag/AgBr/GO-U nanocomposite, adsorption capacity and charge transfer were increased and the efficiency of the electron–hole separation was also encouraged. As the results indicated that the sample synthesized via

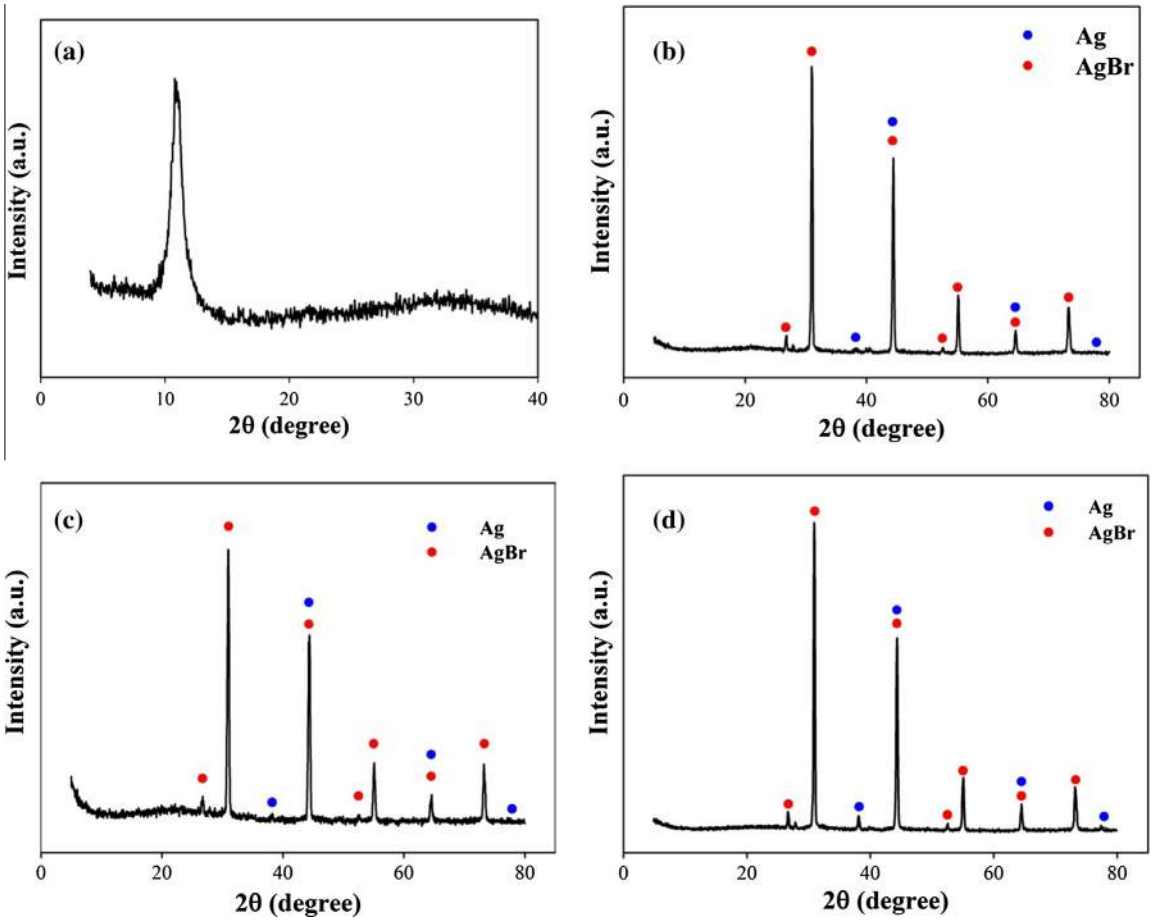

Fig. 4. XRD spectrum of (a) GO, (b) Ag/ABr, (c) Ag/ABr/GO-C and (d) Ag/AgBr/GO-U.

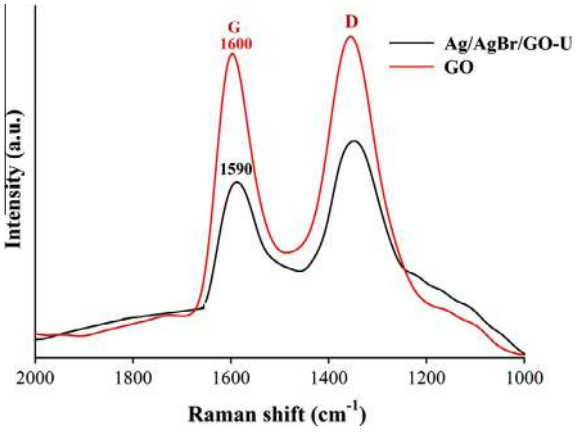

Fig. 5. Raman spectra of Ag/AgBr/GO-U and GO.

ultrasound method showed higher photocatalytic activity than the sample synthesized via classic method, therefore, total experiments performed with the ultrasonic sample (Ag/agBr/GO-U).

Fig. 8a presents the effect of GO loading with different value of GO in the composition of the samples prepared by ultrasound (0, 0.5 and 1 mg ml^{-1}) on the degradation of MO. The catalyst with 0 mg ml^{-1} of GO (Ag/AgBr) exhibited the lowest activity, while the Ag/AgBr/GO-U nanocomposite with 1 mg $ml^{-1}$of GO showed the highest adsorption and activity in comparison with other composites. Therefore, the photocatalytic activity can be improved by adding a small quantity of GO which can enhanced specific surface area and adsorption capacity, speed up the separation of photogenerated electrons and holes on Ag/AgBr and an increase of charge transfer when Ag/AgBr/GO-U nanocomposite are excited with light. Fig. 8 shows the photocatalytic activities of the synthesized samples under different conditions.

Fig. 8(b–d) shows the UV–Vis absorption graphs of MO (10 mg/L^{-1}, 50 mg/L^{-1}) in the presence of Ag/AgBr/GO-U photocatalyst under sunlight irradiation. It can be seen that the MO decreased considerably as the process time increased. According to change of the absorbance intensity at 464 nm (Fig. 8(b and c)), the decolorization efficiency of MO solutions (10 mg L^{-1}) in the presence of Ag/AgBr/GO-U photocatalyst reached to 70% and 100%, respectively after 2 min. Decolorization of MO solution (50 mg L^{-1}, Fig. 8d) needed more time that is associated with the more MO molecules with constant amount of ag/AgBr/GO-U nanocomposite.

3.3. Adsorption isotherm

One of the important factors in photocatalytic process is the amount of pollutant adsorption on the surface of catalyst. Therefore, indicating adsorption isotherm, maximum of adsorbed dye on surface of catalyst and other related factors seems necessary. As the catalyst is active with exposure on the light, the adsorption isotherm was performed in the dark place. For this purpose, different aqueous solution of MO with different initial concentration and 0.015 g catalyst were stirred in dark to attain equilibrium. The concentration of MO after 15 min (equilibration period) was determined with UV–vis spectrophotometer and the amount of adsorbed MO was calculated by using the following equation:

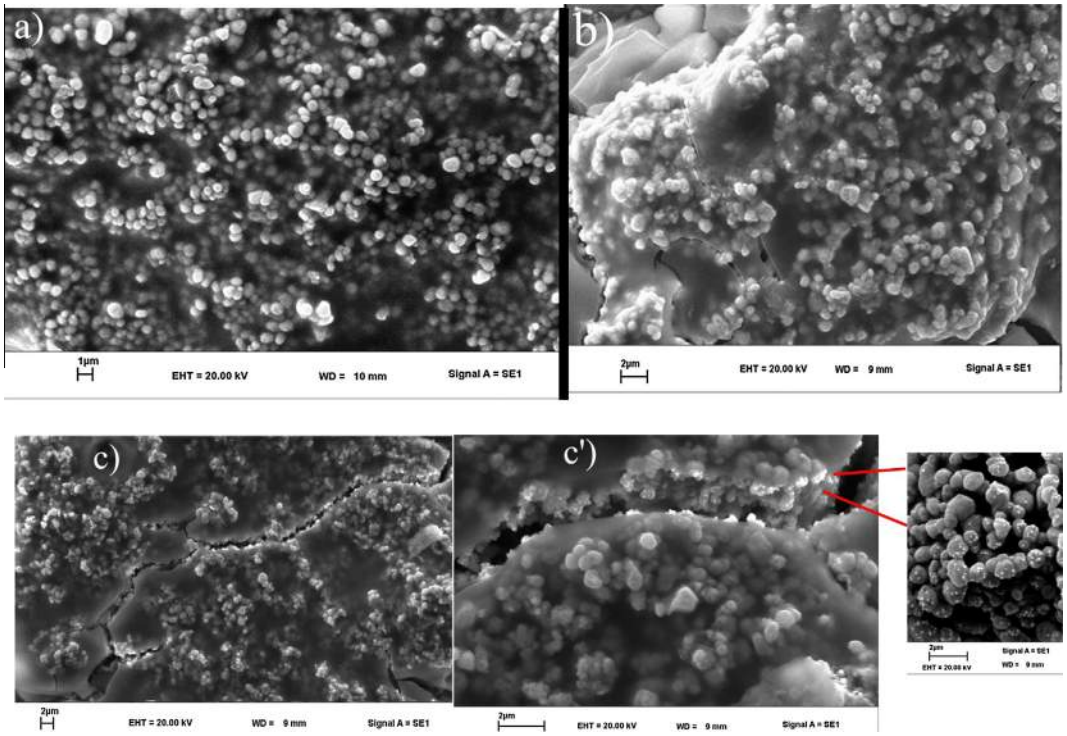

Fig. 6. SEM images of (a) Ag/AgBr, (b) Ag/AgBr/GO-C, (c) and (c′) Ag/AgBr/GO-U at low and high magnification respectively.

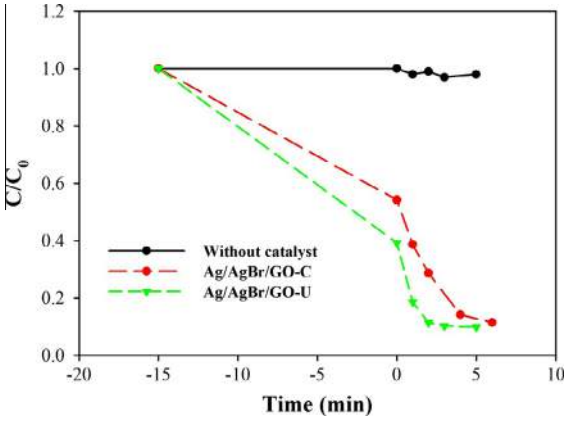

Fig. 7. Solar photocatalytic performance of Ag/AgBr/GO-C and Ag/AgBr/GO-U in degradation of MO.

$$q_e = \frac{v(C_0 - C_e)}{W} \quad (1)$$

where v is the volume of the solution of MO (L), C_0 is the initial concentration of MO (ppm), C_e is the equilibrium concentration of MO (ppm) and W is the weight of the nanocatalyst (g), and q_e presents the amount of adsorbed dye at equilibrium (mg g^{-1}). All calculated adsorption data were established to fit the Langmuir isotherm as in the following equation:

$$\frac{C_e}{q_e} = \left(\frac{1}{q_{max}K}\right) + \left(\frac{1}{q_{max}}\right)C_e \quad (2)$$

where C_e is the equilibrium concentration of MO after 15 min, q_e is the adsorbed MO concentration on the photocatalyst surface at equilibrium, q_{max} (mg g^{-1}) is the maximum amount of dye adsorbed on the catalyst and K (L mg^{-1}) is the equilibrium constant. Based on the Langmuir isotherm (Fig. 9), the obtained values of the Langmuir parameters are showed in Table 1.

The Ag/AgBr/GO with GO = 1 mg ml^{-1} exhibited higher adsorption at dark due to larger specific surface area that is appropriate for high photodegradation of dye on the surface of catalyst.

3.4. Photocatalytic degradation

Activity of the Ag/AgBr/GO-U nanocomposites were tested during the solar degradation of MO and compared with Ag/AgBr/GO-C. Desorption of non-degraded species (dye molecules) on the surface of the catalyst were calculated too. According to Fig. 10, the synthesized Ag/AgBr/GO-U showed higher photocatalytic activity than the Ag/AgBr/GO-C under solar light. Its higher activity can be attributed to the higher specific surface area due to smaller size of sheets and particles, more adsorption capacity and more efficient separation of photoinduced hole–electron pairs in the nanocomposite during the transfer of charge by graphene oxide nanosheets. It was observed that the concentration of MO in solution decreased continuously with time (Fig. 10) and achieved almost to 100% of removal from solution in 6 min, 15 min and 30 min in Ag/AgBr/GO-U (GO = 1 mg mL^{-1}), Ag/AgBr/GO-U (GO = 0.5 mg mL^{-1}) and Ag/AgBr/GO-C (GO = 0.5 mg mL^{-1}), respectively. The degradation on the surface of catalyst was done under solar light irradiation and was completed after 15 min, 30 min and 45 min by the mentioned nanocomposites with the same order, respectively. The desorption results of Ag/AgBr/GO-U (GO = 1 mg mL^{-1}) indicate that the adsorbed MO remaining on the surface of catalyst after 6 min is about 80%. Therefore, the photocatalytic decomposition was required up to 15 min to degrade the MO on the catalyst surface. On the other hand, in the case of Ag/AgBr/GO-U (GO = 0.5 mg ml^{-1}) nanocomposite, desorption results indicate the adsorbed MO remaining on the catalyst surface after 10 min is about 85%. This result indicated the key role of GO

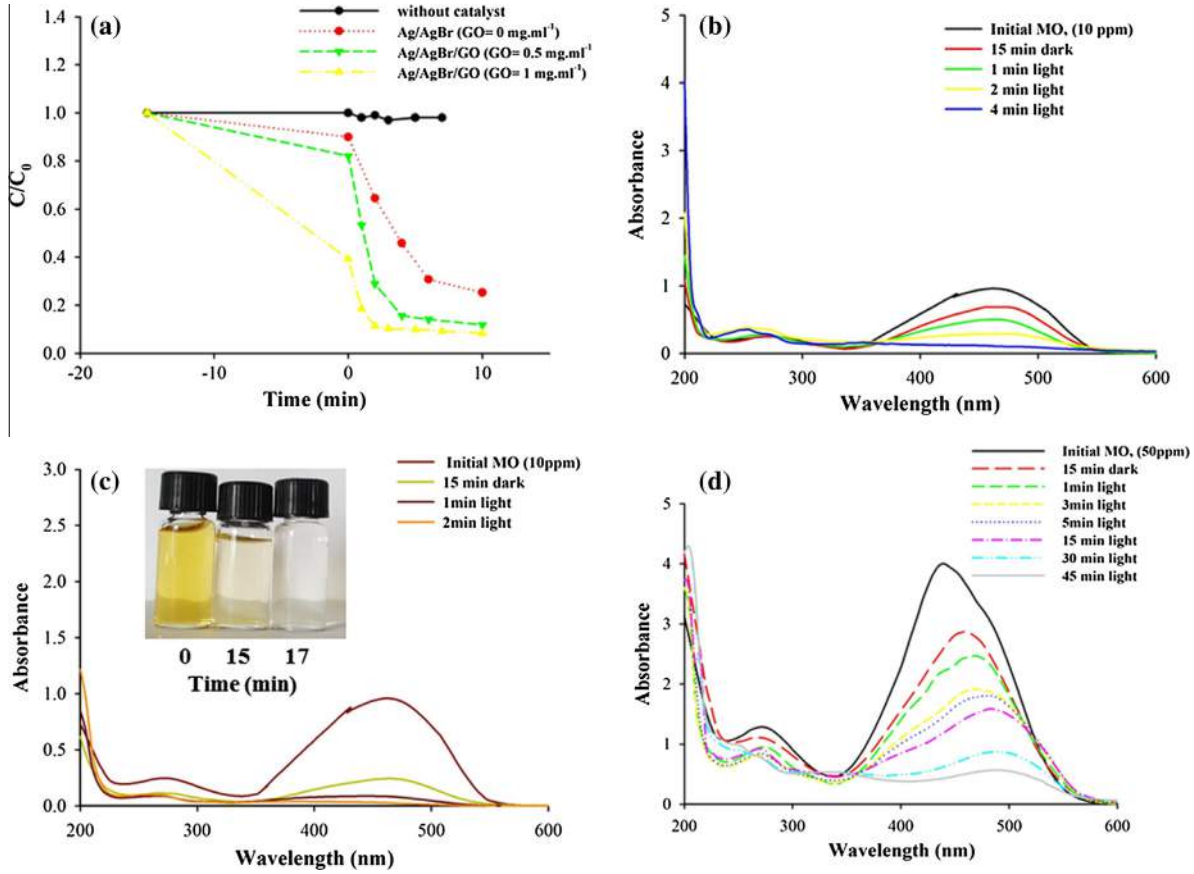

Fig. 8. (a) Photocatalytic activity of Ag/AgBr/GO-U in MO degradation with different values of GO in composite. UV–Vis absorption spectra of (b) MO 10 ppm solution at different contact times with Ag/AgBr/GO-U, GO = 0.5 mg ml^{-1}, (c) MO 10 ppm solution at different contact times with Ag/AgBr/GO-U, GO = 1 mg ml^{-1}, inset: the color change of MO during the process and (d) MO 50 ppm solution at different contact times with Ag/AgBr/GO-U, GO = 1 mg ml^{-1}.

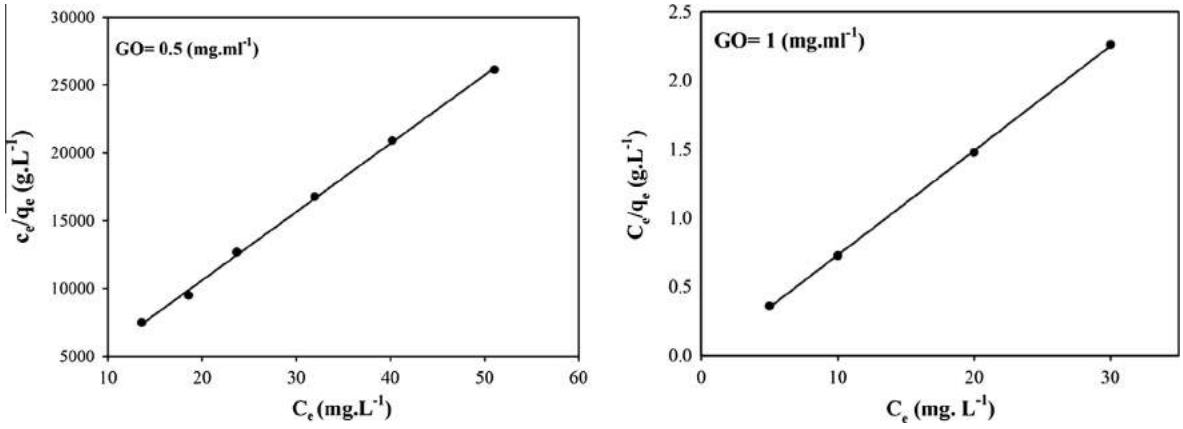

Fig. 9. Langmuir isotherms of MO adsorption on Ag/AgBr/GO-U with different values of GO.

Table 1
Langmuir parameters for Ag/AgBr/GO-U as photocatalysts.

Catalyst	K (L mg^{-1})	q_{max} (mg g^{-1})	R^2
Ag/AgBr/GO-U-0.5	0.97	1.98	0.99
Ag/AgBr/GO-U-1	0.15	20.28	0.98

in photocatalytic activity because of high specific surface area and enhanced charge transfer on GO nanosheet surface.

The real degradation percent obtained via the following equation:

$$\%Real\ Degradation = \left[\frac{C_0 - (C_t + C_d)}{C_0}\right] \times 100 \quad (3)$$

where C_o, C_t, C_d are the concentration of MO (ppm) at first, at time t in the solution, and at time t on the surface of catalyst that could be desorbed, respectively. The mineralization of MO during photocatalytic process was determined by measuring the COD at different interval time through the process. Fig. 10d shows the COD changes of MO solution during the sunlight irradiation with Ag/AgBr/GO-U (GO = 0.5 mg ml^{-1}). In 10 min of irradiation, 50% of COD was decreased and when time of sun irradiation increased to 30 min, the COD reached to about zero. In fact, the adsorption and

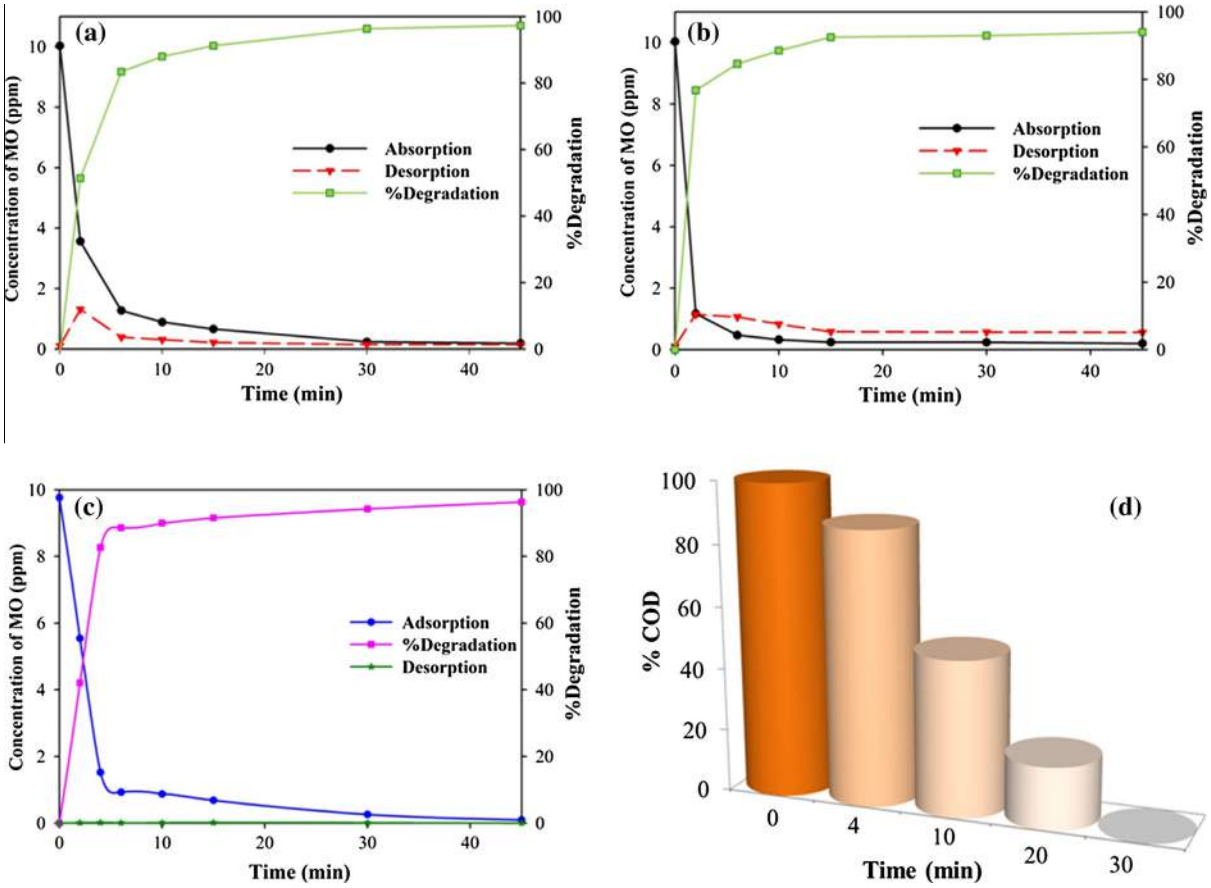

Fig. 10. Adsorption, desorption and degradation percent of the MO solution versus time in the presence of (a) Ag/AgBr/GO-U-0.5, (b) Ag/AgBr/GO-U-1 and (c) Ag/AgBr/GO-C-0.5 under solar light irradiation and (d) COD of MO solution in the presence of Ag/AgBr/GO-U-0.5, (25 mL solution 10 ppm, 0.015 g catalyst).

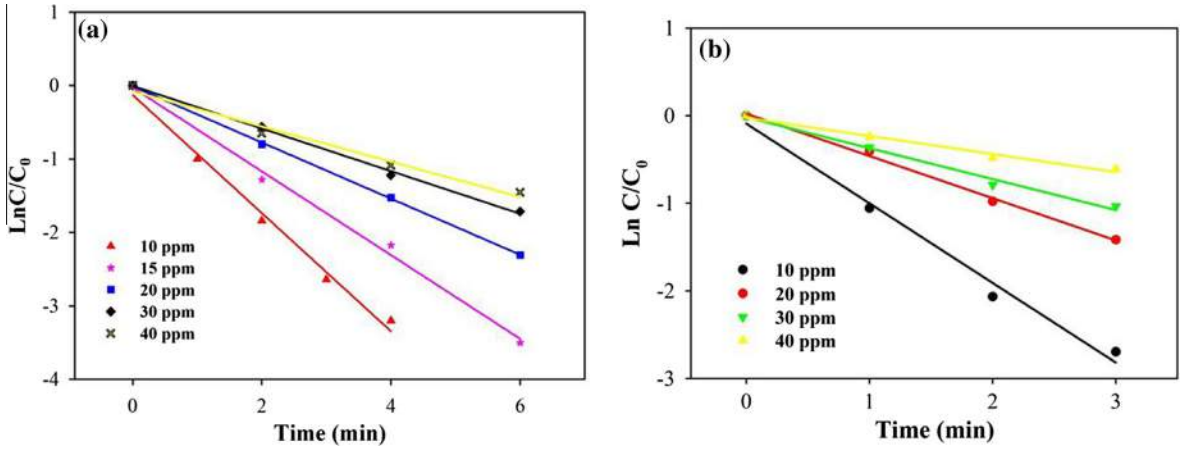

Fig. 11. Photocatalytic degradation kinetics of (a) Ag/AgBr/GO-U-0.5 and (b) Ag/AgBr/GO-U-1.

degradation of MO were performed simultaneously in sun light irradiation. The dye molecules that existence in solution is replaced on catalyst surface when the dye on the catalyst sites decomposed to inorganic species under sunlight irradiation. This process is continued until the whole adsorbed MO is decomposed.

3.5. Kinetics of photocatalytic degradation

To investigate the kinetic of MO degradation, several MO solutions with different initial concentration (10 mg L^{-1}, 15 mg L^{-1}, 20 mg L^{-1}, 30 mg ml^{-1}, 40 mg L^{-1}) were prepared with Ag/AgBr/GO nanocomposites that synthesized in two different values of GO. As shown in Fig. 11. To evaluate the rate constant of MO degradation, Langmuir–Hinshelwood model was used by the following equation:

$$r = -\left(\frac{dC}{dt}\right) = \frac{k_r K C}{1 + KC} \tag{4}$$

where r (mg L^{-1} min^{-1}) is degradation rate, k_r (mg L^{-1} min^{-1}) is rate constant, K (L mg^{-1}) is adsorption coefficient of the pollutant,

Table 2
Kinetic parameters of Ag/AgBr/GO-U nanocomposites.

C_0 (ppm)	Ag/AgBr/GO-U-0.5		Ag/AgBr/GO-U-1	
	k (min^{-1})	R^2	k (min^{-1})	R^2
10	0.8040	0.99	0.910	0.99
20	0.382	0.99	0.481	0.99
30	0.290	0.99	0.353	0.99
40	0.239	0.98	0.206	0.98

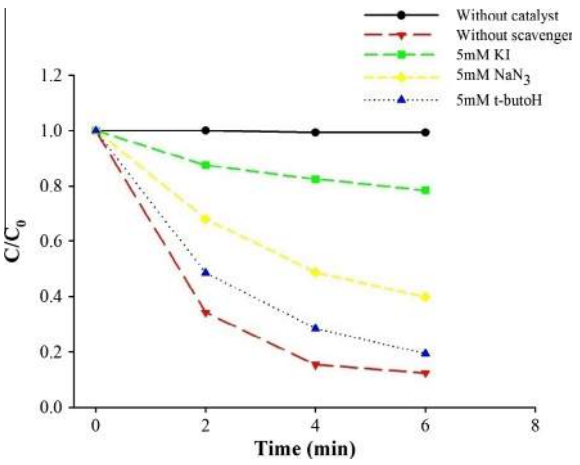

Fig. 12. Effect of different scavengers on the photocatalytic activity of Ag/AgBr/GO-U (GO = 0.5 mg mL^{-1}) nanocomposite on MO degradation.

C (mg L^{-1}) and t (min) are the concentration of MO and time of illumination, respectively. When concentration (C) is very small, Eq. (4) can be changed to the following equation:

$$r = -\left(\frac{dC}{dt}\right) = k_r KC = kC \tag{5}$$

In this equation, k (min^{-1}) is the first-order rate constant. With assuming $t = 0$, $C = C_0$, Eq. (5) can be converted to the following equation:

$$\ln\frac{C}{C_o} = -(Kt) \tag{6}$$

where C_0 and C are the initial concentration and the summation of solution and surface concentrations of MO at every time. The surface concentration was calculated by desorption process. The results showed the photocatalytic degradation is obeyed from first-order kinetics based on the Langmuir–Hinshelwood model. The rate constants were obtained by assuming pseudo-first-order reaction kinetics [47].

The graph of y versus solar irradiation time (t) showed a straight line and through its slope the rate constant of MO degradation can be determined (Fig. 11, Table 2). The rate constant of photocatalytic degradation of MO is higher when the initial concentration is lower, this result exhibited the significant effect of initial concentration of MO on the rate of degradation. This could be described with the finite amount of active sites on the photocatalyst, and the excessive molecules of MO in the solution leads to a reduction in the light absorption ability of the catalyst. Therefore, the photocatalytic process is affected by the initial concentration of MO. In addition, at the same solar irradiation time, the relative amount of MO decomposed is higher for the sample synthesized with more GO content than lower GO content. This is related to the effect of GO nanosheets and their specific surface area.

3.6. Proposed mechanism of MO degradation

Some experiments were considered to indicate the mechanism of MO degradation via Ag/AgBr/GO-U nanocomposite. At first, one experiment was performed on an aqueous MO solution under solar light without catalyst. The result showed that MO was stable versus light irradiation without catalyst. To more investigating the effect of active species, two separate experiments were carried out in the absence and presence of scavengers in the solution, under applied conditions. As it is shown in Fig. 12, after adding of KI as a scavenger of OH· and positive hole, the degradation rate of MO was strongly inhibited. After addition of NaN_3 as a scavenger of superoxide radicals, OH· and electrons, the rate of degradation was decreased too. This result suggests that the degradation of MO were mainly done by the hole, O_2^{-} and ·OH. To confirm the role of ·OH, t-butyl alcohol as a scavenger of ·OH was added to the solution. Based on Fig. 12, by addition of t-butyl alcohol, the rate of degradation was decreased and it means that hydroxyl radical has effect in MO degradation [48,49].

Based on the results obtained, Fig. 13 shows a possible photocatalytic mechanism for the Ag/AgBr/GO nanocomposites under

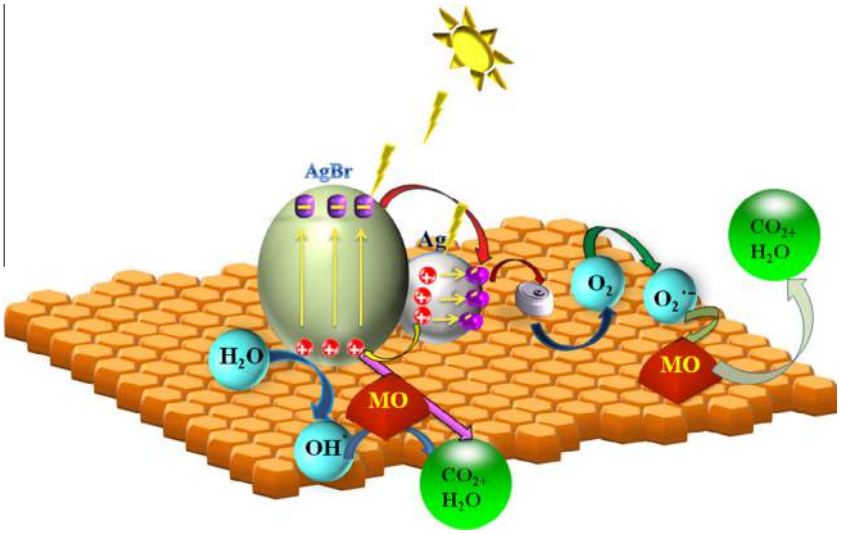

Fig. 13. Possible photocatalytic mechanism of Ag/AgBr/GO nanocomposite.

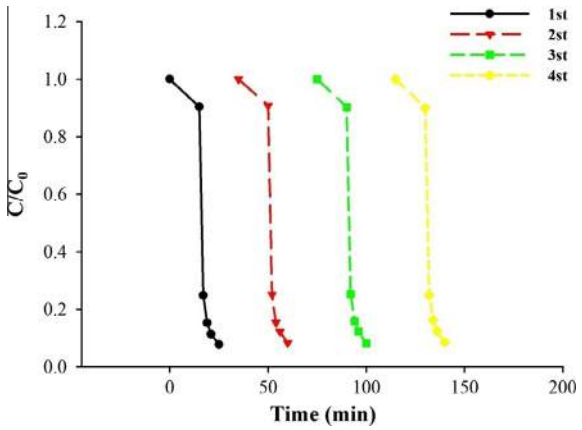

Fig. 14. Photocatalytic degradation of MO in successive cycles by Ag/AgBr/GO-U (GO = 0.5 mg mL^{-1}).

visible light irradiation, both Ag and AgBr nanoparticles can fabricate photogenerated electrons and holes. Generally, the majority of holes and electrons rapidly recombine with each other and only a fraction of them participate in the photocatalytic degradation process, resulting in low quantum efficiency [50]. In the presence of GO, the electrons from Ag and AgBr nanoparticles can be transferred to GO, and then combine with adsorbed oxygen to produce reactive superoxide radicals ($O_2^{\cdot-}$), which is a strong oxidant species to degrade MO molecules. In addition, the reaction of H_2O and holes produce ·OH, and both $O_2^{\cdot-}$and ·OH radicals can degrade organic dyes (MO) efficiently under visible light irradiation. Also, reactive holes at the valance band of Ag and AgBr are able to oxidize organic dye straightly. Therefore, Ag/AgBr/GO composite exhibited higher photocatalytic activity than Ag/AgBr. It is noticeable that the MO molecules were excited by the absorption of sun light, and electrons were injected into the conduction band of AgBr or the Ag nanoparticles and simplifying the oxidation of the MO molecules [51]. The enhanced photocatalytic activity of Ag/AgBr/GO composites should be attributed to the efficient charge separation and fast transfer in the presence of GO nanosheets (see Fig. 13).

3.7. Stability of the catalyst

To investigate the photocatalytic stability of Ag/AgBr/GO, the catalyst was used in a cyclic degradation process four times. In each time, after using, Ag/AgBr/GO nanocomposite was separated from the solution with centrifuge. Then, the collected sample frequently used in successive cycles. In each cycle, Ag/AgBr/GO nanocomposite (0.015 g) was added to 25 mL dye. As it is shown in Fig. 14, MO was quickly decomposed in every cycle. This result indicates that there is no considerable loss of activity even after four cycles. It is confirmed that the Ag/AgBr/GO nanocomposite was stable and active in successive cycles.

4. Conclusion

In summary, the unique and highly efficient visible-light plasmonic photocatalyst based on Ag/AgBr/GO nanocomposite was synthesized via an ultrasonic method at room temperature and short time. The enhanced photocatalytic activity and high stability of the synthesized samples are the interesting points of this work. Ag/AgBr/GO-U nanocomposites showed a high adsorption capacity to MO molecules due to small sizes of particles and GO nanosheets. In addition, the intercalation of nanoparticles between GO layers in ultrasonic sample caused an enhancement in its photocatalytic activity. The amount of GO in nanocomposite affects the photocatalytic activity through changing the adsorption capacity, charge transfer and suppressing recombination of electron–hole pairs in Ag/AgBr/GO. MO was completely degraded in 15 min, 30 min and 45 min with Ag/AgBr/GO-U(GO = 1 mg ml^{-1}), Ag/AgBr/GO-U (GO = 0.5 mg ml^{-1}), and Ag/AgBr/GO-C(GO = 0.5 mg ml^{-1}), respectively. Therefore, the key point of this work is to achieve a nanophotocatalyst via a facile and fast way, with the highest photocatalytic activity and having a complete mineralization of MO under solar light. Achieving these properties was owing to the high pressure and temperature created through the cavitation process that led to the formation of Ag/AgBr/GO nanocomposites with suitable contact surfaces. The photocatalytic degradation mechanism of MO on Ag/AgBr/GO nanocomposite could be preceded via direct reactions of MO with holes trapped on the surface and oxidation of MO with $O_2^{\cdot-}$and ·OH. The experimental data exhibited that the photocatalytic degradation of MO by Ag/AgBr/GO nanocomposite were apparent first-order kinetics based on the Langmuir–Hinshelwood model. The photocatalyst was stable and active under sun light irradiation four following cycle uses.

Totally, the excellent photocatalytic performance, simplicity of the process, complete degradation in ambient conditions by using ultrasound irradiation energy source can be considered as advantages of ultrasonic method.

Acknowledgements

The support of Ferdowsi University of Mashhad – Iran (Research and Technology) for this work (code 3/29791, date 26/01/2014) is appreciated.

References

[1] M. Deo, D. Shinde, A. Yengantiwar, J. Jog, B. Hannoyer, X. Sauvage, M. More, S. Ogale, J. Mater. Chem. 22 (2012) 17055–17062.
[2] P. Shi, R. Su, S. Zhu, M. Zhu, D. Li, S. Xu, J. Hazard. Mater. 229 (2012) 331–339.
[3] X. Chang, G. Yu, J. Huang, Z. Li, S. Zhu, P. Yu, C. Cheng, S. Deng, G. Ji, Catal. Today 153 (2010) 193–199.
[4] N. Daneshvar, S. Aber, M.S. Dorraji, A. Khataee, M. Rasoulifard, Sep. Purif. Technol. 58 (2007) 91–98.
[5] Y. Zhao, L. Kuai, B. Geng, Catal. Sci. Technol. 2 (2012) 1269–1274.
[6] X. Chen, S.S. Mao, Chem. Rev. 107 (2007) 2891–2959.
[7] S. Bingham, W.A. Daoud, J. Mater. Chem. 21 (2011) 2041–2050.
[8] A. Charanpahari, S. Umare, R. Sasikala, Appl. Surf. Sci. 282 (2013) 408–414.
[9] J. Hou, C. Yang, Z. Wang, S. Jiao, H. Zhu, Appl. Catal. B 129 (2013) 333–341.
[10] Y.-G. Lin, Y.-K. Hsu, Y.-C. Chen, S.-B. Wang, J.T. Miller, L.-C. Chen, K.-H. Chen, Energy Environ. Sci. 5 (2012) 8917–8922.
[11] P. Zhang, C. Shao, X. Li, M. Zhang, X. Zhang, Y. Sun, Y. Liu, J. Hazard. Mater. 237 (2012) 331–338.
[12] X. Zhou, G. Liu, J. Yu, W. Fan, J. Mater. Chem. 22 (2012) 21337–21354.
[13] P. Wang, B. Huang, Y. Dai, M.-H. Whangbo, Phys. Chem. Chem. Phys. 14 (2012) 9813–9825.
[14] J.-F. Guo, B. Ma, A. Yin, K. Fan, W.-L. Dai, J. Hazard. Mater. 211 (2012) 77–82.
[15] S.K. Cushing, J. Li, F. Meng, T.R. Senty, S. Suri, M. Zhi, M. Li, A.D. Bristow, N. Wu, J. Am. Chem. Soc. 134 (2012) 15033–15041.
[16] P. Gao, K. Ng, D.D. Sun, J. Hazard. Mater. 262 (2013) 826–835.
[17] Y. Li, Y. Ding, J. Phys. Chem. C 114 (2010) 3175–3179.
[18] P. Wang, B. Huang, Z. Lou, X. Zhang, X. Qin, Y. Dai, Z. Zheng, X. Wang, Chem.-a Eur. J. 16 (2010) 538–544.
[19] D. Wang, Y. Duan, Q. Luo, X. Li, L. Bao, Desalination 270 (2011) 174–180.
[20] H. Xu, H. Li, J. Xia, S. Yin, Z. Luo, L. Liu, L. Xu, ACS Appliedmater. Interfaces 3 (2010) 22–29.
[21] L. Liu, H. Xu, H. Li, Y. Xu, J. Xia, S. Yin, J. Phys. Chem. Solids 73 (2012) 523–529.
[22] Y. Xu, H. Xu, J. Yan, H. Li, L. Huang, J. Xia, S. Yin, H. Shu, Colloids Surf., A 436 (2013) 474–483.
[23] Y. Xu, H. Xu, J. Yan, H. Li, L. Huang, Q. Zhang, C. Huang, H. Wan, Phys. Chem. Chem. Phys. 15 (2013) 5821–5830.
[24] W. Cui, H. Wang, Y. Liang, B. Han, L. Liu, J. Hu, Chem. Eng. J. 230 (2013) 10–18.
[25] P. Wang, B. Huang, Q. Zhang, X. Zhang, X. Qin, Y. Dai, J. Zhan, J. Yu, H. Liu, Z. Lou, Chem.-A Eur. J. 16 (2010) 10042–10047.
[26] L. Zhang, K.-H. Wong, Z. Chen, C.Y. Jimmy, J. Zhao, C. Hu, C.-Y. Chan, P.-K. Wong, Appl. Catal. A 363 (2009) 221–229.
[27] Q. Xiang, J. Yu, M. Jaroniec, Chem. Soc. Rev. 41 (2012) 782–796.
[28] P. Wang, Y. Tang, Z. Dong, Z. Chen, T.-T. Lim, J. Mater. Chem. A 1 (2013) 4718–4727.
[29] M. Zhu, P. Chen, M. Liu, Langmuir 29 (2013) 9259–9268.

[30] M. Zhu, P. Chen, M. Liu, ACS Nano 5 (2011) 4529–4536.
[31] J. Balapanuru, J.X. Yang, S. Xiao, Q. Bao, M. Jahan, L. Polavarapu, J. Wei, Q.H. Xu, K.P. Loh, Angew. Chem. 122 (2010) 6699–6703.
[32] H. Wang, H.S. Casalongue, Y. Liang, H. Dai, J. Am. Chem. Soc. 132 (2010) 7472–7477.
[33] Y. Wang, L. Sun, B. Fugetsu, J. Mater. Chem. A 1 (2013) 12536–12544.
[34] M. Zhu, P. Chen, M. Liu, Langmuir 28 (2012) 3385–3390.
[35] F. Nacimiento, R. Alcántara, U.G. Nwokeke, J.R. González, J.L. Tirado, Ultrason. Sonochem. 19 (2012) 352–357.
[36] M. Arenas, L.F. Rodríguez-Núnez, D. Rangel, O. Martínez-Álvarez, C. Martínez-Alonso, V. Castaño, Ultrason. Sonochem. 20 (2013) 777–784.
[37] P. Rouhani, N. Taghavinia, S. Rouhani, Ultrason. Sonochem. 17 (2010) 853–856.
[38] J.H. Bang, K.S. Suslick, Adv. Mater. 22 (2010) 1039–1059.
[39] A. Esmaeili, M. Entezari, J. Colloid Interface Sci. 432 (2014) 19–25.
[40] C. Zeng, M. Guo, B. Tian, J. Zhang, Chem. Phys. Lett. 575 (2013) 81–85.
[41] X.-H. Meng, X. Shao, H.-Y. Li, J. Yin, J. Wang, F.-Z. Liu, X.-H. Liu, M. Wang, H.-L. Zhong, Mater. Lett. 105 (2013) 162–165.
[42] J. Bartram, R. Ballance, Water Quality Monitoring: a Practical Guide to the Design and Implementation of Freshwater Quality Studies and Monitoring Programmes, CRC Press, 1996.
[43] P. Wang, B. Huang, X. Zhang, X. Qin, H. Jin, Y. Dai, Z. Wang, J. Wei, J. Zhan, S. Wang, Chem.-A Eur. J. 15 (2009) 1821–1824.
[44] P. Wang, B. Huang, X. Qin, X. Zhang, Y. Dai, J. Wei, M.H. Whangbo, Angew. Chem. Int. Ed. 47 (2008) 7931–7933.
[45] L. Kuai, B. Geng, X. Chen, Y. Zhao, Y. Luo, Langmuir 26 (2010) 18723–18727.
[46] L. Zhou, W. Wang, S. Liu, L. Zhang, H. Xu, W. Zhu, J. Mol. Catal. A: Chem. 252 (2006) 120–124.
[47] J. Xu, W. Wang, M. Shang, S. Sun, J. Ren, L. Zhang, Appl. Catal. B 93 (2010) 227–232.
[48] G. Li, J. Qu, X. Zhang, H. Liu, H. Liu, J. Mol. Catal. A: Chem. 259 (2006) 238–244.
[49] T. Soltani, M.H. Entezari, Chem. Eng. J. 223 (2013) 145–154.
[50] J. Yu, W. Wang, B. Cheng, B.-L. Su, J. Phys. Chem. C 113 (2009) 6743–6750.
[51] W. Teng, X. Li, Q. Zhao, J. Zhao, D. Zhang, Appl. Catal. B 125 (2012) 538–545.